1	Compensation state and geophysical evolution of Sputnik Basin on Pluto	
2		
3	S.A. Moruzzi ¹ , J.C. Andrews-Hanna ¹ , A. Broquet ² , P. Schenk ³	
4		
5	¹ Lunar and Planetary Laboratory, University of Arizona, Tucson, AZ, ² Institute for Planetary	
6	Research, German Aerospace Center, DLR, Berlin, Germany, ³ The Lunar and Planetary	
7	Institute/USRA, Houston, TX.	
8	Corresponding Author: Samantha Moruzzi (<u>smoruzzi@arizona.edu</u>)	
9	Key Points:	
10	• Sputnik basin is a filled with low-viscosity N2-ice, which as an equipotential surface, can	
11	be used to calculate the basin's gravity field	
12	• Sputnik's concave-up topography is consistent with a largely uncompensated basin and a	
13	mass deficit today	
14	• Sputnik basin may have transitioned from a past mass excess to a present-day mass	
15	deficit via refreezing of the uplifted subsurface ocean	
16		
17		
18		
19		
20		
21		
22		
23		

Abstract

24

25

26

27

28

29

30

31

32

33

34

35

36

37

38

39

40

41

42

43

44

45

46

Sputnik basin is an ~2000 × 1000 km elongated impact basin located in the equatorial region of Pluto. It contains a low-viscosity N₂-rich ice deposit that has prompted comparisons between Sputnik basin and mascon basins in the inner Solar System – some of which were initially isostatically compensated by the uplift of high-density mantle materials in the subsurface and evolved to a mass excess from the lithospheric support of infilling material. In the absence of gravitational data, novel approaches must be considered to examine the structure of Sputnik basin. Here, we assume that the surface of the low-viscosity infill conforms to Pluto's geoid, and we use this constraint to evaluate the local gravity field over the basin considering a range of ice shell thicknesses and N₂-deposit thicknesses. Our results show that an isostatically compensated pre-fill Sputnik basin has a strongly negative free-air gravity anomaly due to the attenuation of the gravity signature through Pluto's relatively thick ice shell compared to mean radius. The best fit models to Sputnik basin reflect a present-day mass deficit and a largely uncompensated basin, which is at odds with previous work suggesting a past mass excess and overcompensated basin. To reconcile these, we propose that the substantially thinned post-impact ice shell beneath the basin was out of thermal equilibrium, leading to the refreezing of the uplifted ocean and to the basin transitioning to a present-day mass deficit. This new evolutionary pathway has important implications for Pluto's interior structure and the evolution, and longevity, of a subsurface ocean.

Plain Language Summary

Sputnik basin is a unique feature in the outer Solar System and the basin's structure provides insight into the subsurface of Pluto. The present-day equilibrium state of the basin, the thickness of the ice shell beneath the basin, and the thickness of the nitrogen ice inside the basin are currently unknown but could be revealed by the gravity field. The New Horizons mission to Pluto did not measure the gravitational signature of Sputnik. Thus, we used a novel approach by assuming the low-viscosity nitrogen ice filling the basin follows an equipotential surface, like sea level on Earth, revealing the gravity field and enabling us to constrain the basin structure. Such an approach has been widely used over oceans on Earth and here it allows us to evaluate the gravitational signature of Sputnik on Pluto. Our analyses indicate that at present-day Sputnik basin is out of equilibrium, suggesting that the ice shell beneath the basin may have refrozen over time. The results of this work have implications for the possible existence and longevity of a subsurface ocean on Pluto.

1. Introduction

The New Horizons flyby of Pluto in 2015 revealed numerous surface features, with Sputnik basin being the dominant feature on the encounter hemisphere. This ~2000×1000 km quasi-elliptical basin is located in Pluto's equatorial region, and its elongated shape reflects the expected shape of large basins formed by an oblique impact on a curved surface (Andrews-Hanna, 2010; Moruzzi et al., 2023; Ballantyne et al., 2024). The basin has a present-day depth of ~2.5 km and, unlike large impact basins on other outer Solar System objects, is partially filled with an N₂-ice-rich volatile deposit known as Sputnik Planitia (henceforth referred to as the N₂-layer, Stern et al., 2015; Schenk et al., 2018; McKinnon, et al., 2016; Keane et al., 2016; Nimmo

et al., 2016). A polygonal pattern observed on the surface of the N₂-layer has been interpreted to represent underlying convection cells (McKinnon et al., 2016; Trowbridge et al., 2016). The maximum N₂-layer thickness estimated from the size of these convection cells ranges from 3–11 km, depending on the assumed horizontal-to-vertical aspect ratio of the convection cells (Moruzzi et al., 2023). The present-day shape of the basin floor does not show evidence of significant viscous relaxation (Schenk et al., 2016). Sputnik basin, combined with the N₂-layer within it, is a unique feature in the outer Solar System, more closely resembling giant impact basins in the inner Solar System (Moruzzi et al., 2023). As with basins on the Moon and Mars (e.g., Johnson et al., 2018; Searls et al., 2006), the structure of Sputnik basin may reveal important information about the formation and evolution of the basin, as well as the evolution of Pluto itself. As such, the N₂ filled Sputnik basin provides an example of how large surface landforms can be used to understand planetary interiors, especially in data-limited environments such as Pluto.

Gravity anomalies of impact basins have been integral sources for understanding the subsurface structure of the basins themselves, the processes responsible for their formation, and the interior structure of their host bodies (e.g., Andrews-Hanna, 2013; Freed et al., 2014; Johnson et al., 2018). However, the New Horizons mission did not gather any spatially resolved gravitational data, so innovative approaches are needed to shed light on Pluto's subsurface structure. Modeling studies have provided scenarios of Sputnik's formation and structure, but direct constraints from geophysical data have been lacking. For example, previous work suggested that the Sputnik-forming impact resulted in gravity-driven collapse accompanied by a flow of ice and underlying ocean towards the basin center, leading to the uplift of that underlying ocean (Johnson et al., 2016; Nimmo et al., 2016). Thus, the basin would most likely have been

approximately isostatically compensated by a high-density ocean layer (i.e., in a state of vertical equilibrium between the lighter ice shell and the denser ocean) and transitioned to a mass excess upon loading by the N₂-layer (Keane et al., 2016; Nimmo et al., 2016; Johnson et al., 2016). The basin's present-day location suggests Sputnik realigned with Pluto's tidal axis through true polar wander, resulting in a stress field that is consistent with the orientation of the tectonics surrounding the basin (Keane et al., 2016), supporting the inference of a mass excess in the basin. However, the present-day compensation state, the amount of subsurface uplift of the underlying ocean, the lithospheric strength of the ice shell, and the depth to the ice-ocean interface beneath the basin remain unknown.

The inferred positive mass anomaly within Sputnik basin would provide support for the presence of a subsurface ocean on Pluto. However, the present-day compensation state is unknown. Gravity data is required to constrain compensation state, which is most commonly expressed in terms of the anomalous acceleration (units of mGal or 10^{-5} m/s²). Geoid anomalies, representing the height of an equipotential surface above a reference spheroid or ellipsoid (units of m) provide another representation of the gravity field, and are useful as they emphasize longer wavelength features, which are particularly relevant for a feature of the scale of Sputnik basin. If Sputnik basin was initially isostatically compensated, we would expect the free-air gravity anomaly and geoid anomaly of the basin to have been weakly negative immediately after the impact. As the basin evolved to an overcompensated state through the lithospheric support of the N₂-layer, the free-air anomaly and geoid would have evolved to positive, and notably stronger, geoid and free-air anomaly values. This process has been inferred and analyzed at basins across the solar system, including at lunar mascons, such as Imbrium and Serenitatis on the Moon, or Isidis basin on Mars. Many mascons exhibit strong positive free-air anomalies resulting from

volcanic infill, though the mantle uplift beneath them may also contribute to the positive free-air anomaly even if the infill is removed (Solomon and Head, 1980; Ritzer & Hauck, 2009; Broquet & Andrews-Hanna, 2023b). As discussed above, the initial isostatic support and transition to a mass anomaly within Sputnik basin would provide support for the presence of a subsurface ocean on Pluto (e.g., Keane et al., 2016; Nimmo et al., 2016). However, if Sputnik basin was instead a present-day mass deficit, it would exhibit a strong, negative geoid and free-air anomaly and require an alternative formation and evolutionary history.

Whether Sputnik basin is a present-day mass excess or deficit affects the interpretation of the evolution of the subsurface. A positive mass anomaly would require the initial isostatic support of the basin (Keane et al., 2016; Nimmo et al., 2016). Liquid water is the most likely compensating material, though a rock-ice mixture is also a possibility (Hammond et al., 2016). A positive mass anomaly/mascon could also be the result of a remnant of the rocky impactor core at the base of the ocean (Ballantyne et al., 2024). In contrast, a present-day mass deficit may be the result of an uncompensated basin in a very thick ice shell (Nimmo et al., 2016), viscous relaxation of the basin (e.g., Kihoulou et al., 2022) or refreezing of the uplifted subsurface ocean after the impact (Hammond et al. 2016). However, as noted above, analyses of the structure and compensation state of basins typically rely on gravity and topography data, the former of which is not available for Pluto.

In this work, we use a novel approach to tackle this problem, the key to which lies in the topography of the N_2 -layer within the basin. This feature is one of the smoothest terrains on the surface of Pluto because it is composed of low-viscosity ices including N_2 ice (Schenk et al., 2018; Moore et al., 2016). N_2 -ice can behave like a viscous fluid at Pluto surface conditions (temperature ~40 K and surface pressure ~10 kPa), with viscosity of ~1.6x10¹⁰ Pa s (Umurhan et

al., 2017). This viscosity is two orders of magnitude less than the viscosity of the solid H₂0 at subfreezing terrestrial conditions of $\sim 10^{12}$ Pa s, but much greater than the typical viscosity of liquid water, at $\sim 10^{-3}$ Pa s, suggesting that N₂-ice under these conditions is expected to flow rapidly over geologic timescales. The deposit surface has a polygonal pattern that has been interpreted as delineating the edges of convection cells (McKinnon et al. 2016; Trowbridge et al., 2016; Moruzzi et al., 2023), further supporting the low viscosity and geologically rapid flow rate of the material. Over long wavelengths, this low-viscosity deposit should follow an equipotential surface, excluding any significant external perturbations, and thus should conform to Pluto's geoid. Therefore, the topography of the N2- layer (Figure 1) can provide us with indirect information on the gravity field within the basin that can be compared to predictions from models of the subsurface structure of the basin (Moruzzi et al., 2024). Previous terrestrial studies have conducted similar analyses utilizing sea surface elevation as a constraint on the geoid (Anderson and Knudsen, 1996; 1998). Therein, satellite altimetry from GeoSAT and ERS-1 was used to detect long-wavelength geoid anomalies beneath Earth's oceans assuming that the lowviscosity liquid water oceans conformed to an equipotential surface such that global sea surface elevation is representative of Earth's geoid. Our approach will be one of the first applications of this principle beyond Earth (see also Kanamaru et al., 2019) because of the unique low viscosity deposit within Sputnik basin. Here, we utilize this approach to constrain the gravity field and geoid anomalies over Sputnik basin, which are compared with predictions from models of the structure and compensation of the basin, thereby constraining the evolution of the interior structure of Pluto through time.

139

140

141

142

143

144

145

146

147

148

149

150

151

152

153

154

155

156

157

158

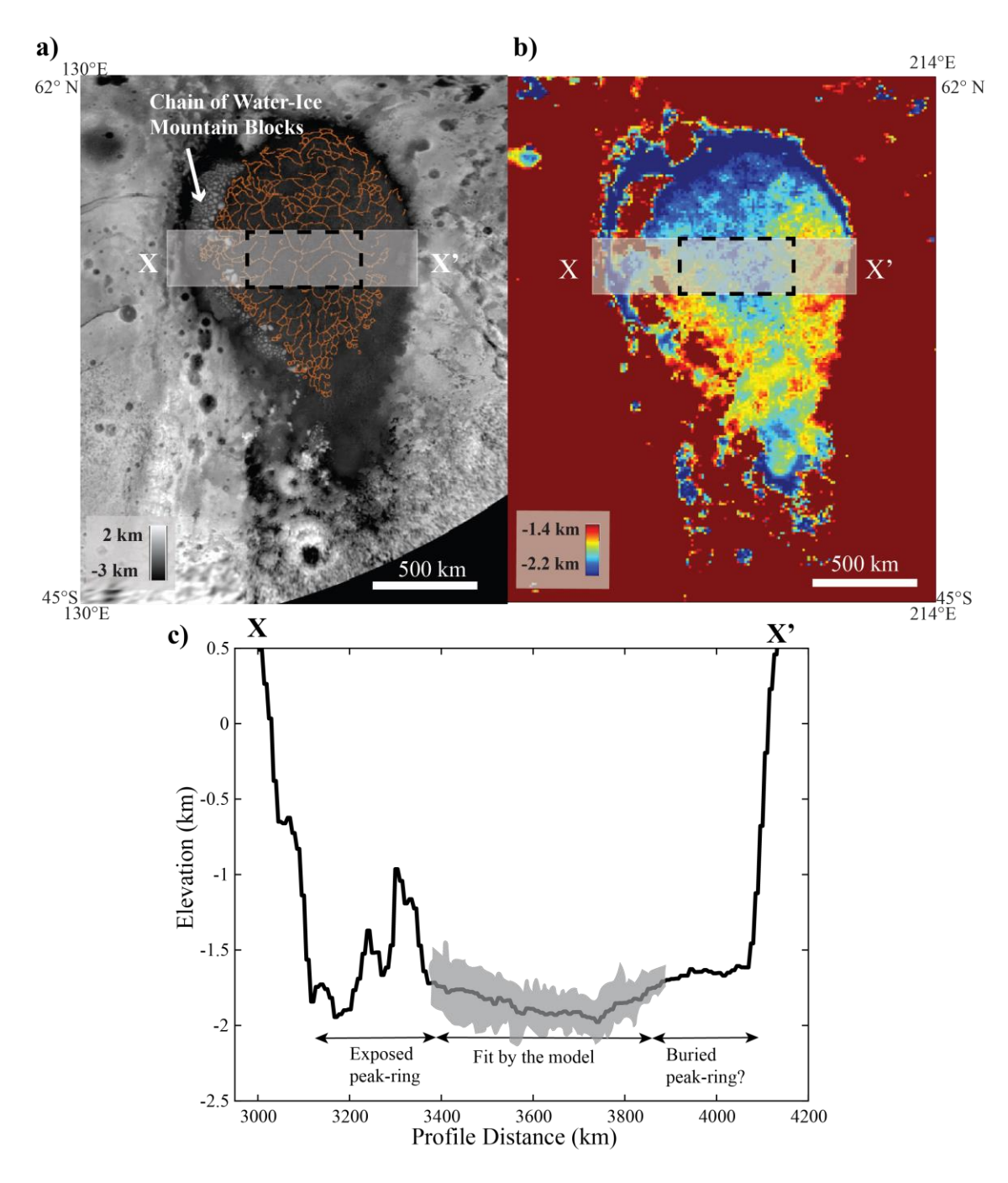


Figure 1. DEM for Sputnik basin in a) grayscale with overlay of polygonal pattern interpreted to be convection cells in orange and b) stretched color-coded altimetry highlighting the relief within Sputnik Planitia. Average profile in c was calculated from east to west profiles across the basin from $15^{\circ} - 30^{\circ}$ N. The grey rectangles in (a) and (b) designate the region from where the profiles were taken from. The gray shaded area in c represents the variation in elevation of the profiles

used for the average profile in the region fit to the models. This region is indicated in map view by the black dashed lines in a and b. The locations of the water-ice mountain blocks interpreted as a possible exposed peak-ring in the western basin, and the inferred buried component in the east are labeled in (a) and (c).

We explore this approach by modeling the present-day state of the basin, taking into account the membrane-flexural deformation of the lithosphere in response to loading within the basin, and comparing the resulting model geoids to the constraint from the N₂-layer (Section 2). We consider a wide parameter space for the ice shell thickness, the thickness of the N₂-layer, and present-day degree of compensation of the basin. The best-fit models for present-day Sputnik basin show a mass deficit and a largely uncompensated basin. While the ice shell thickness and N₂-layer thickness are poorly constrained, models within the preferred ranges of these parameters support a largely uncompensated basin today. If Pluto reoriented to align Sputnik basin's mass excess with the tidal axis in the past, but the basin is a present-day mass deficit, the change in compensation state must be explained. We suggest that the dense subsurface ocean may have refrozen to, or near, the equilibrium thickness, evolving Sputnik basin from an overcompensated state to an uncompensated state.

2. Methods

2.1. Data

We use the topography of Sputnik Planitia as a proxy for Pluto's geoid. The relief of Sputnik Planitia is mapped using the Digital Elevation Model (DEM) created from high resolution images obtained by the New Horizons Long-Range Reconnaissance Imager (LORRI)

and the Multispectral Visible Image Camera (MVIC) at a horizontal resolution of ~300 m/pixel (Figure 1, Schenk et al., 2018; Moore et al., 2016). The shape of the long-wavelength topography represented in the DEM is sensitive to the mean radius input (Schenk et al., 2018). While this is most apparent in the LORRI-LORRI DEMs or strip mosaics, which were not directly utilized in this study, some of the effect may still be present in the global DEM. The MVIC-based DEMs are more strongly affected by a short-wavelength rumpling in the topography, which was smoothed out in the processing of the DEM and further minimized by the orientation of our profiles and the averaging of the profiles (see below). Nevertheless, we acknowledge some uncertainty in the long wavelength topography. Future improvements to the DEM can be compared to our model results to better refine the compensation state of the basin.

We focus our study only on the east-to-west basin profiles, averaging between $15^{\circ}-30^{\circ}$ N (Figure 1). Only east-to-west profiles were utilized because there is a variation in elevation in the north-to-south profiles of ~2 km (Schenk et al., 2018; Bertrand et al., 2018) due to climate-driven sublimation and deposition of the N₂-layer resulting from changes in insolation, thermal inertia, and surface temperature with Pluto's obliquity cycles (Bertrand et al., 2018). This north-south elevation difference matches model predictions of up to ~300 m of N₂-rich ice deposited in the southern regions of the Planitia (<15° N) and up to 1 km of N₂-rich ice sublimated from the northern region (>45° N) during the last obliquity cycle of ~2.8 Myr (Bertrand et al., 2018). There is minimal (<10 m) predicted elevation change due to sublimation/condensation processes east-to-west across the basin and there is also minimal elevation change due to these processes in the central region of the Planitia (~15° N–35° N). Furthermore, profiles north of this range (>35° N) show increased influence of sublimation and northward flow of N₂-ice, with predicted changes in elevation reaching >280 m (Bertrand et al., 2018; Umurhan et al., 2017). Profiles

south of this range (<10° N) show increased influence of the topographic expression of proposed peak-ring, which inhibits our ability to properly compare the geoid models for the peak-ring structure to the average stereo topography across the basin.

215

216

217

218

219

220

221

222

223

224

225

226

227

228

229

230

231

232

233

212

213

214

2.2. Interpretations

For a low-viscosity material such as the N₂-rich ice, any departure from the geoid would require an active process to generate substantial variation in topography. While Sputnik Planitia is one of the smoothest surfaces on Pluto, there are slight topographic variations across the basin. The topography in the average east-to-west profile across the basin floor is dominated by a concave-up shape, with a minimum of -1.95 km in the center of the basin and a maximum of -1.50 km near inner edge of the proposed inner ring (Figure 1). Both the individual profiles and the average profile show this concave-up shape east-to-west across the basin, which is the focus of our study. The east-to-west concave-up shape cannot be explained by glacial flow into the basin as this process only occurs in limited, concentrated areas, accounting for one to two orders of magnitude less spatial area than the basin cross-section (Umurhan et al., 2017; Bertrand et al., 2018). Therefore, any net flow within the basin from the glacial input would be exceedingly slow and should not generate substantial variations in elevation. Additionally, there is no localized substantial relief in areas of glacial flow into the basin. Thus, we assume that the longwavelength structure (>100 km) of the east-to-west profiles across the low-viscosity N₂-layer in the basin conform to an equipotential surface and the topography of the deposit provides information on Pluto's geoid. This framework provides a new constraint on the gravity field within Sputnik basin. With the assumption that the east-to-west topography conforms to Pluto's

geoid, we can use the topography to compare to the predicted geoid over the basin for a variety of scenarios and interior parameters.

2.3. Loading model

The predicted geoid is a function of the lithospheric support of the N₂-layer, the unfilled structure of the basin and its contribution to the load, and the flexural response of the lithosphere to the net load (Turcotte and Schubert, 2002; Johnson et al., 2018; McGovern et al., 2021). Our model considers a net load from the combined effects of the unfilled basin topography, the N₂-layer inside the basin, and the relief along the base of the ice shell. While the exposed basin topography and N₂-layer thickness are directly inferred from observations, the subsurface structure of the basin must be assumed.

We consider two approaches for modeling the present-day subsurface structure of Sputnik basin, with one representing a giant impact basin and the second a peak-/multiring basin (Figure 2). Giant impact basins such as Hellas on Mars are characterized by one primary topographic ring interpreted as the rim, and crustal thinning extending beneath the entirety of the basin interior to the rim, although minor rings have been identified interior and/or exterior to the primary rim in some cases (e.g. Potter et al., 2015). If Sputnik is analogous to these giant impact basins, the shell thinning and any potential mascon would stretch across the entire basin interior. However, more recent work suggests that Sputnik basin is morphologically and topographically consistent with peak-/multiring basins in the inner Solar System (Moruzzi et al., 2023), with the north-south trending chain of water-ice mountain blocks exposed in the western half of the basin representing the inner ring. Peak-/multiring basins are basins with two or more topographic rings with crustal thinning confined within the inner ring, such as Hertzsprung or Orientale on the

Moon (Johnson et al., 2018; Bjonnes et al., 2023). If Sputnik basin is a peak-/multiring basin, the subsurface structure of the ice shell may resemble the subsurface crustal structure of peak-ring basins in the inner Solar System (Neumann et al., 2013; Wieczorek and Phillips, 1998), and any central ocean uplift or potential mascon would be confined within the inner ring. The potential ring structure of Sputnik affects its subsurface structure and gravity signature.

The giant impact basin model considers Sputnik basin analogous to Hellas basin on Mars, with the central ocean uplift being confined within the main topographic rim and extending beneath the entirety of the basin floor similar to the mantle uplift below Hellas (Neumann et al., 2004). For the giant impact basin interpretation, we represent the pre-loading interior of Sputnik basin as flat-floored, which provides a reasonable representation based on the flat floor of the similarly sized Hellas and Utopia impact basins on Mars (Searls et al., 2006; Neumann et al., 2004). The entire basin is assumed to be isostatic prior to infilling, as expected for giant impact basins (Trowbridge et al., 2020). We assume the present-day lithosphere supports the load within the basin, and the thickness of the N₂-layer is determined from the depth of the pre-loading basin and the response of the lithosphere to the load. As with the central ocean uplift beneath the basin, the N₂-layer extends to the main topographic rim (Figure 2).

The peak-/multiring model considers Sputnik basin with a central ocean uplift confined within the proposed inner ring bounded by the N-S trending chain of water ice mountain blocks in the west and the furthest extent of the convection cells within the basin in the east (Moruzzi et al., 2023; Figure 2). The putative inner ring may continue circumferentially within Sputnik basin despite the lack of topographic expression, as it may be buried beneath the fill in the eastern and northern quadrants of the basin. Thus, in this model the central shell thinning, pre-fill topographic depression, and mass concentration are much narrower and may be expected to

result in a more concave geoid. For the peak-/multiring interpretation, we use the unloaded basin shape derived in Moruzzi et al. (2023), using the diameters of the polygonal pattern interpreted as convection cells (McKinnon et al., 2016) expressed in the N₂-layer to constrain the fill thickness.

280

281

282

283

284

285

286

287

288

289

290

291

292

293

294

295

296

297

298

299

300

301

302

Lunar basins show that, apart from any mare infilling, the basin floor of peak-/multiring basins can range from isostatic to super-isostatic (a mascon) typically surrounded by a subisostatic annulus and thicker crust/shell between the inner and outer rings (Andrews-Hanna, 2013; Melosh et al., 2013; Freed et al., 2014). The thickened part of the crust due to ejecta may be removed through viscous relaxation for basins on the lunar nearside due to the higher heat flow (Ding & Zhu, 2022). Thus, the inner part of Sputnik basin is assumed to be surrounded by a sub-isostatic annulus with a thick, but depressed, shell between the main topographic rim and the inner ring, similar to basins such as Freundlich-Sharonov on the Moon (Neumann et al., 2015). We defined the shell-ocean interface for two structural endmembers: a topographically flat annulus between the inner and outer rings and an annulus of constant shell thickness. In the latter case, the base of the shell is translated downwards beneath the low elevation annulus between the outer ring and inner ring as observed for the base of the crust around lunar basins. For simplicity, we do not consider an annulus of thickened shell due to the impact ejecta surrounding the basin as observed around some lunar basins, but models including this effect would increase the magnitude of the positive geoid anomaly predicted for the basin and be rejected.

We modeled the Sputnik gravitational signature from the topography and assumed subsurface structure using a thin-shell deformation model (Broquet & Andrews-Hanna, 2023a, 2023b; Broquet et al., 2022) based on a prior model used to invert gravity and topography data (Banerdt, 1986; Beuthe, 2008). For the maximum elastic lithosphere thickness considered of 150

km, the thin-shell approximation is acceptable on Pluto for modeling features at spherical harmonic degrees <15 or horizontal scales >470 km (Beuthe et al., 2008) and thus is appropriate for analysis of Sputnik basin. The model solves a system of equations relating the topography, variations in the undeformed relief along the base of the crust or shell, the geoid at the surface, the geoid at the base of the crust, the flexure of the lithosphere, the vertical load on the lithosphere, the tangential load arising from variations in topography, and internal density variations. If three of these parameters are specified, the rest can be solved self-consistently. For example, if gravity and topography are known and internal density variations are assumed to be zero, it is possible to solve for the combinations of crustal loads and resulting flexure (e.g., Banerdt 1986; Banerdt & Golombek, 1990; Andrews-Hanna et al., 2008). Alternatively, assumptions regarding the interior load and lithospheric response can be used to predict both gravity and topography (e.g., Broquet & Andrews-Hanna 2023b). Here, we use the known topography and assumptions regarding the loads associated with the basin structure and fill to calculate the gravity. The model allows for loading at multiple interfaces and considers variations in gravity with depth and the added load from geoid relief along density interfaces.

303

304

305

306

307

308

309

310

311

312

313

314

315

316

317

318

319

320

321

322

323

324

325

The gravity and topography of the present-day basin have been influenced by the pre-fill basin structure and the N₂-layer surface load. We define the pre-fill basin as the basin structure after the basin excavation and modification stages and prior to infilling of any N₂-rich ice. To represent the pre-fill topography and basal interface, we first use estimated N₂-layer thicknesses (Moruzzi et al., 2023) to model the deformation of the base of the ice shell. We then remove the N₂-layer and associated deformation to define the pre-fill topography and assume isostasy to retrieve the pre-fill shell-ocean interface relative to the pre-fill topography. Our modeling approach defines isostasy as the state leading to zero vertical displacement, also known as zero

deflection isostasy (Banerdt, 1986; Beuthe et al., 2021). Isostasy can also be defined as the condition that minimizes stress in the lithosphere (minimum stress isostasy; Beuth et al., 2021). Zero deflection isostasy and minimum stress isostasy produce identical isostatic ratios under the thin-shell approximation used here and only differ slightly under other conditions (Beuthe et al., 2016; Beuthe et al., 2021). In the context of Sputnik basin, zero deflection isostasy is simpler to implement within our modeling approach. Within our model, this definition of isostasy considers the effects of the curvature of the planet, the change in gravity with depth, membrane stresses, the horizontal load potential, and the contribution to the net load from the geoid anomalies at the surface and subsurface density interfaces (Banerdt, 1986). We quantitatively investigate these contributions to determine their effect on the isostasy of the basin. The models then test range of unfilled/unloaded compensation states for the basin center, from fully uncompensated (degree of compensation DOC = 0) to overcompensated (DOC = 1.5), defining isostasy as DOC = 1. We define the unfilled basin as the basin without the full N₂-layer thickness within it. Unless otherwise noted, the DOC refers to the basin in its unfilled/unloaded state. We then add the N₂layer back into the model as a load to represent the present-day basin.

We compare the modeled geoid to the observed topography of Sputnik Planitia. Best fitting models and parameter ranges are evaluated using the root-mean-square (RMS) misfit between the average topographic profiles across the basin and the average profiles of the geoid models to determine the best fitting ranges of these parameters. Since our approach is sensitive to the relative shape of equipotential surface and geoid rather than the radius of the equipotential surface, each profile is shifted vertically to minimize the misfit for any one combination of parameters.

326

327

328

329

330

331

332

333

334

335

336

337

338

339

340

341

342

343

344

345

346

2.4. Assumed elastic and structural parameters

349

350

351

352

353

354

355

356

357

358

359

360

361

362

363

364

365

366

367

368

369

370

371

In order to place constraints on the structural parameters (Figure 2), we incorporate a range in N_2 -layer thicknesses making up the load inside Sputnik basin (L) and vary the ice shell thickness (T_s) and elastic lithosphere thickness (T_e) of Pluto at the time of loading. N₂-layer thickness is measured convection cell dimensions within the N₂-layer, which tend to be larger in the basin center and decrease outward to near 0 km at the edge of the water-ice mountain blocks/potential peak-ring (Moruzzi et al., 2023), and preferred aspect ratios of 4–6 (McKinnon et al., 2016; Moruzzi et al., 2023). Previous studies suggest that too thin of a layer (≤3 km) might hinder convection, while an overly thick N₂-layer (≥10 km) would lead to a mass concentration inconsistent with Pluto's reorientation (Keane et al., 2016; Nimmo et al., 2016). We test a range of maximum N₂-layer thicknesses from 3–10 km following the methodology of Moruzzi et al. (2023). This range also includes the load thicknesses of ~4–8 km required to reorient Pluto to its present location through true polar wander if the basin was initially isostatic (Keane et al., 2016), and load thicknesses of < 6 km favored by loading and flexural models of the basin (McGovern et al., 2021). Thus, our preferred N₂-layer thickness range is 4–9 km, but values out of this range are also tested for completeness.

The loading models are highly dependent on the ice shell and elastic thickness at the time of loading, with ice shell thickness being greater than the elastic thickness. The elastic thickness governs response to the loading, while the ice shell thickness governs the attenuation of the gravity anomaly arising at the ice-ocean interface, We test a range of present-day ice shell thicknesses outside the basin from 80–300 km, which spans the range considered in impact modeling (Johnson et al., 2016; Denton et al., 2023), loading and tectonic models (Conrad et al., 2019; McGovern et al., 2021; Schmidt and Salvini, 2024) and thermal modeling of the ice shell

(Hammond et al., 2016; Bierson et al., 2018). We consider a preferred range of 165 – 265 km based on previous thermal model studies (Robuchon & Nimmo, 2011; Hammond et al., 2016; Bierson et al., 2018). An ice shell greater than 265 km may result in dense ice II at depth, which would lead to compressional tectonics at the surface that are not observed (Hammond et al., 2016). We note that the present-day geoid reflects the present-day ice shell thickness, while the response to the loading reflects the lithosphere thickness at the time of loading (likely reflecting a combination of effects spanning in age from the impact to the present-day). As shown below, our geoid models are more sensitive to ice shell thickness than to elastic thickness, so we establish the range in ice shell thickness first.

The relationship between the elastic thickness of the ice shell and the ice shell thickness depends on the assumed thermal conductivity profile within the ice shell and, less strongly, on the assumed heat flux. The base of the elastic lithosphere is assumed to correspond to a temperature of 120 K, above which ice loses most of its yield strength and has a relatively high viscosity (Bierson et al., 2018, Robuchon & Nimmo, 2011). We apply a 1D explicit finite difference thermal model to a fully conductive ice shell. We adopt a surface heat flux of 3 mW/m², which is scaled for the heat flux at the base of the shell to account for the varying radius of the ice-ocean interface with time, but the results are not strongly sensitive to this assumption. The base of the ice shell corresponds to the assumed melting temperature of 250 K. For all test cases, the elastic thickness at equilibrium is 42–55% of the ice shell, so we adopt an intermediate value of 50% (Figure S1). Tests of our model framework confirm that the resulting gravity anomaly is more dependent on the ice shell thickness rather the elastic thickness (Figure S2).

Giant Impact Basin - - - - - Peak-ring basin

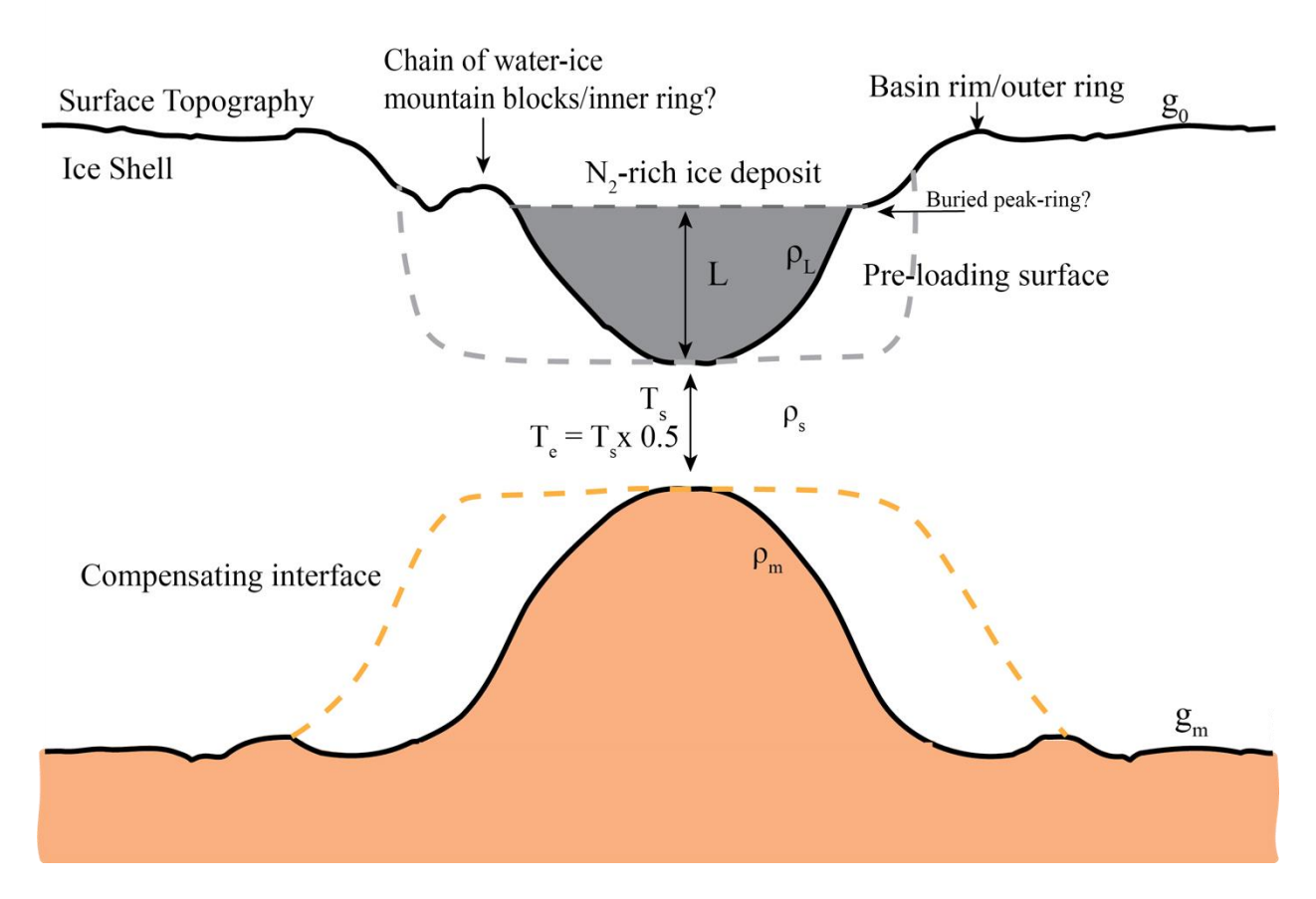


Figure 2. Cross-sectional schematic of Sputnik basin for the both the giant impact and peak-multiring basin scenarios. Important interior parameters are defined and symbols definition can be found in Table 1. Schematic is not to scale.

We focus on a density contrast across the basal interface of 80 kg/m³, corresponding to a pure water-ice shell (920 kg/m³) above a liquid water ocean (1000 kg/m³) (Nimmo et al., 2016; Johnson et al., 2016). We use a density of 1000 kg/m³ for the N_2 -layer within the basin (Stern et al., 2015; Nimmo et al., 2016). We assume Young's modulus of 9×10^9 Pa for pure water-ice

(Nimmo et al., 2003) and Poisson's ratio of 0.33, but our results are not strongly sensitive to the assumptions for these parameters. The parameters utilized in the model are listed in Table 1.

Table 1. Key Parameters for Membrane-Flexural and Geoid Modeling

Parameter	Value
Mean Pluto density (ρ)	1860 kg/m ³ (Stern et al. 2015)
N_2 -layer density (ρ_l)	1000 kg/m ³ (Nimmo et al., 2016)
Ocean density (ρ_m)	1000 kg/m ³ (Nimmo et al., 2016)
Ice shell density (ρ_s)	920 kg/m³ (Nimmo et al., 2016
Young's modulus (E)	9×10 ⁹ Pa (Nimmo et al., 2003)
Surface gravity (g_0)	0.62 m/s^2
Poisson's ratio (v)	0.33
Mean planetary radius (R)	1188.3 km (Nimmo et al., 2017)
Ice shell thickness (T_s)	80–300 km (e.g. Hammond et al., 2016)
Elastic/lithospheric thickness (T_e)	$0.5 \times T_s (40 - 150 \text{ km})$
N_2 -layer thickness (L)	3-10 km (Moruzzi et al., 2023)
Degree of Compensation (DOC)	0–1.5

2.5. Model evaluation

408

409

410

411

412

413

414

415

416

417

418

419

420

421

422

423

To constrain best-fit ranges in the parameters discussed above, we set a series of criteria by which we evaluate the fit of the modeled geoids compared to the observed topography of the low-viscosity N₂-ice layer. Models are evaluated based on the RMS misfit between the predicted geoid profile and the observed average topographic profile across Sputnik Planitia. Rather than focus on a single best-fit model, we use a t-test to identify the range of best-fit models that have misfits that are statistically indistinguishable from the overall best-fit model for a particular scenario at the 95% confidence level. An equal variance t-test is appropriate as the populations of misfits are approximately normally distributed and have nearly the same variance. We then utilize the variation in the average topographic profile to determine an allowable range of models. We calculate the standard error of the average topographic profile as a function of distance along the profile and use the RMS standard error as a measurement of data uncertainty. This value is then compared to the RMS misfit between the average topographic profile and the profile of each modeled geoid. Models with RMS misfit values within 1 standard error of the data are considered allowable models. Finally, our preferred models also exist within the allowable and best-fit ranges but are based on the preferred range of N₂-layer thicknesses and shell thicknesses as defined above.

425

426

427

428

429

430

424

3. Results

3.1. Models of the pre-fill compensated basin

We first model Sputnik basin as an isostatically compensated (DOC = 1), preloaded/unfilled basin. Our nominal case removes a 6-km-thick N_2 -layer inside the basin, assuming a 200 km ice shell thickness (corresponding to an elastic thickness of 100 km). We start with the giant impact hypothesis due to its structural simplicity. The gravity field is here discussed in terms of the more commonly used free air anomaly in mGal, though the geoid is used for comparison of the final models with the relief of Sputnik Planitia. Our model shows that an isostatically compensated unfilled basin at Sputnik's scale has a strongly negative free-air gravity anomaly of -175 mGal (Figure 3). The free-air gravity over the basin is strongly sensitive to ice shell thickness, ranging from -225 mGal for a shell thickness of 200 km to -125 mGal for a shell thickness of 100 km (Figure 3). This trend can be explained by the fact that depthattenuation of gravity from the compensating interface is less important for thinner shells (Banerdt, 1986). The free-air gravity is also influenced by the thickness of the removed N₂-layer, which changes the pre-fill basin depth, ranging from -250 mGal for a N₂-layer thickness of ~9 km and an ~11 km pre-fill basin depth to -70 mGal for a N₂ thickness of ~3 km and an ~4 km pre-fill basin, assuming a shell thickness of 150 km (Figure S3). The free-air gravity anomaly within the basin center is less strongly negative than the anomaly just inside the rim of the basin, expressed by a concave-down shape in the center of the basin (Figure 3) due to the dominant effect of attenuation of the short wavelength gravity anomalies from the base of the shell with increasing radius. However, the geoid anomaly is dominated by the longer wavelengths and is concave upward for these isostatic basins.

431

432

433

434

435

436

437

438

439

440

441

442

443

444

445

446

447

448

449

450

451

452

453

This strongly negative gravity anomaly for the isostatic basin, in contrast to the weak anomalies for similar basins on terrestrial bodies, is largely a result of the attenuation of the positive anomaly from the uplift of the ice-ocean interface, owing to its great depth below the surface relative to the radius of Pluto. Pluto's relatively small radius and somewhat thick ice shell results in a strong attenuation of the gravity anomaly from the compensating interface when upward continued to the surface. As a result, even in the simple scenario in which the mass or

pressure anomalies exactly cancel, a strong negative gravity and geoid anomaly would be observed at the surface (Figure S4). For basin dimensions of 1000–2000 km corresponding to degrees 4–7, the gravity anomaly from the base of a 200-km-thick ice shell would be attenuated by 40–60% when upward continued to the surface, leaving a strong negative anomaly for the unfilled basin. The inclusion of these contributions into investigations of compensation will be important for other icy outer Solar System objects, especially those with larger shell thicknesses compared to their mean planetary radius, such as Charon (Conrad et al., 2019).

The change in gravitational acceleration with depth (Sleep & Phillips, 1979; Dahlen et al., 1982; Hemingway & Matsuyama, 2017), the contribution of the geoid to the net load, and the horizontal load potential also play a role in the gravity anomaly, though the attenuation of the positive gravity anomaly from the uplifted ocean is the dominant effect. The effect of the change in gravitational acceleration with depth may be small on Earth, but it can be an important factor on a smaller object, where the crust/shell is a substantial fraction of the mean radius (Hemingway & Matsuyama, 2017). For a differentiated Pluto, g increases by $\sim 10\%$ at a depth of 200 km, requiring slightly less relief on the compensating interface. For the case of an isostatically compensated impact basin, the contribution of changes in gravity with depth increase the magnitude of the free-air anomaly, pushing towards a more negative anomaly.

Geoid anomalies at the surface and ice-ocean interface have an effect similar to deflections of these interfaces and thereby contribute to the net vertical load. The horizontal load potential includes the effects of horizontal pressure gradients to the vertical load. To quantify the contributions of the different components of our model to the isostatic gravity anomaly, we first consider the non-physical scenario of zero shell thickness, thereby removing the effect of the attenuation of gravity anomalies with depth and the variation of g with radius. In this scenario,

the combined effects of the contribution of the geoid to the vertical load and of the horizontal load potential lead to a weak positive gravity anomaly of \sim 17 mGal (Figure S5). Removing the effect of the geoid brings the gravity anomaly down to 12 mGal, and removing the horizontal load potential as well reduces the gravity anomaly to 0 mGal. Next, we take a shell thickness of 150 km and similarly turn off the effects of the contribution of the geoid to the load and the horizontal load potential, finding that they contribute 10-15% and 20-30% of the total gravity anomaly for this scenario (Figure S6). These two effects are both of the same order as the effect of the variation of g with radius (Figure S7), and they partially cancel the negative anomaly arising from the attenuation of gravity with radius.

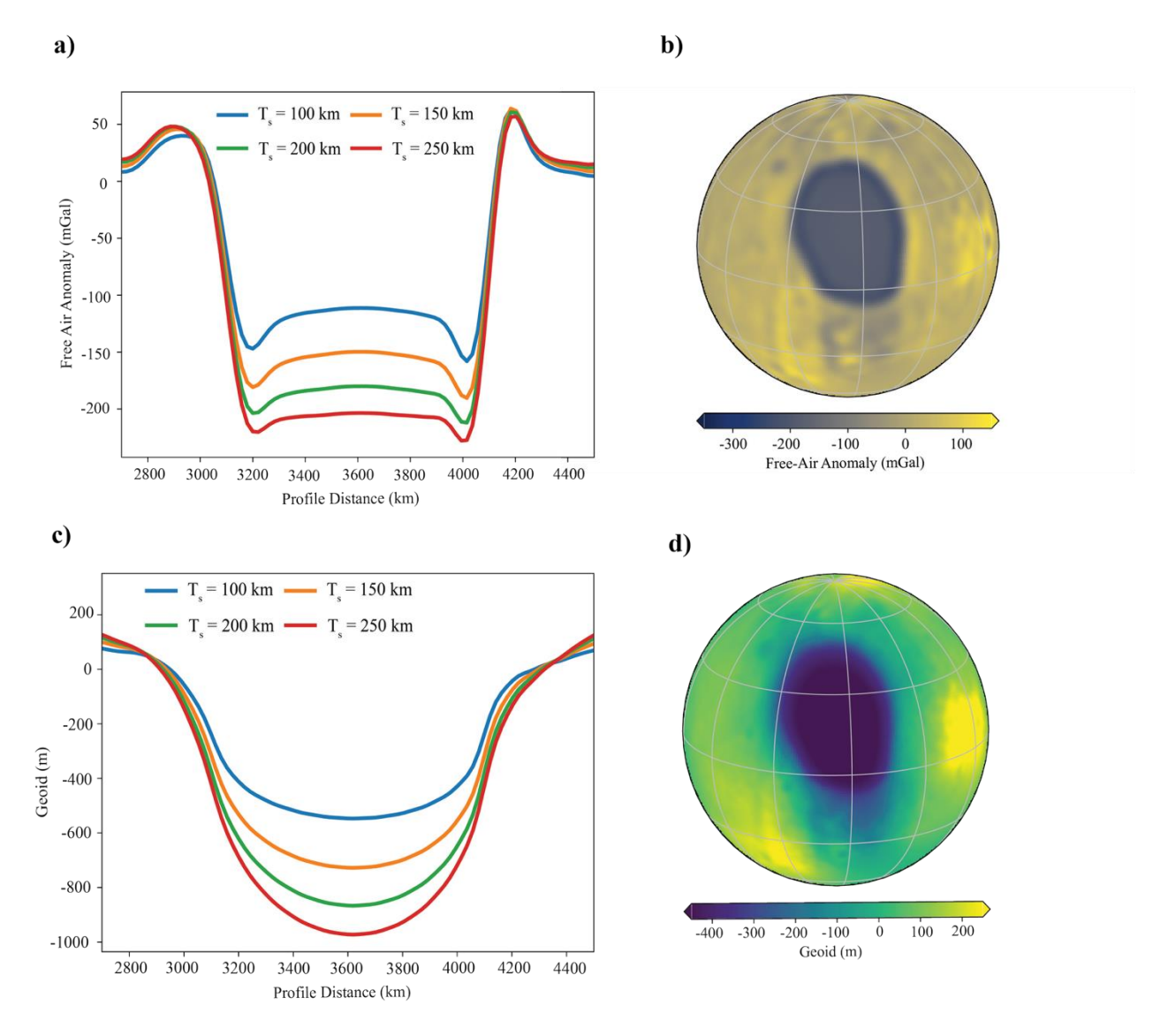


Figure 3. a) Free-air gravity anomaly and c) geoid anomalies across a pre-fill, isostatically compensated Sputnik basin (DOC=1) for shell thickness (T_s) of 100 km (blue), 150 km (orange), 200 km (green), 250 km (red). The N₂ deposit thickness L is kept constant at 6 km in determining the pre-fill structure. Orthographic projection of free-air gravity anomaly (b) and geoid (d) across a pre-fill, isostatically compensated Sputnik basin for $T_s = 200$ km, L = 6 km.

3.2. Models of the present-day basin structure

The geoid over present-day Sputnik basin is controlled by the degree of compensation (DOC) of the pre-fill basin, shell thickness, and N₂-layer thickness. The gravity and geoid anomaly for an initially compensated pre-fill basin become positive once the fill thickness is added back in as a load supported by the lithosphere. The qualitative results from visually comparing cross-sectional profiles of the geoid models to the observed topography of Sputnik Planitia for both structural cases (giant impact basin and peak-/multi-ring basin) show that an under-compensated unloaded basin with a degree of compensation of <0.5 is required for a concave up geoid on the basin floor after filling (Figure 4). The two models are nearly identical for the uncompensated case (DOC=0), whereas the difference in influence of the giant impact basin structure versus the peak-ring structure on the geoid is better observed in the overcompensated models. For both basin structure models, geoid models corresponding to nearly compensated (DOC> 0.5) to over-compensated pre-fill basins (i.e., with a central mascon gravity anomaly and DOC> 1) after the addition of the fill are concave down in shape and do not match the topography of the N₂-layer. However, in some cases, models corresponding to nearly compensated basins with large shell thicknesses can provide reasonable fits to the topography with a weakly concave upward geoid. These results support a present-day mass deficit over the basin and an under-compensated pre-fill basin.

496

497

498

499

500

501

502

503

504

505

506

507

508

509

510

511

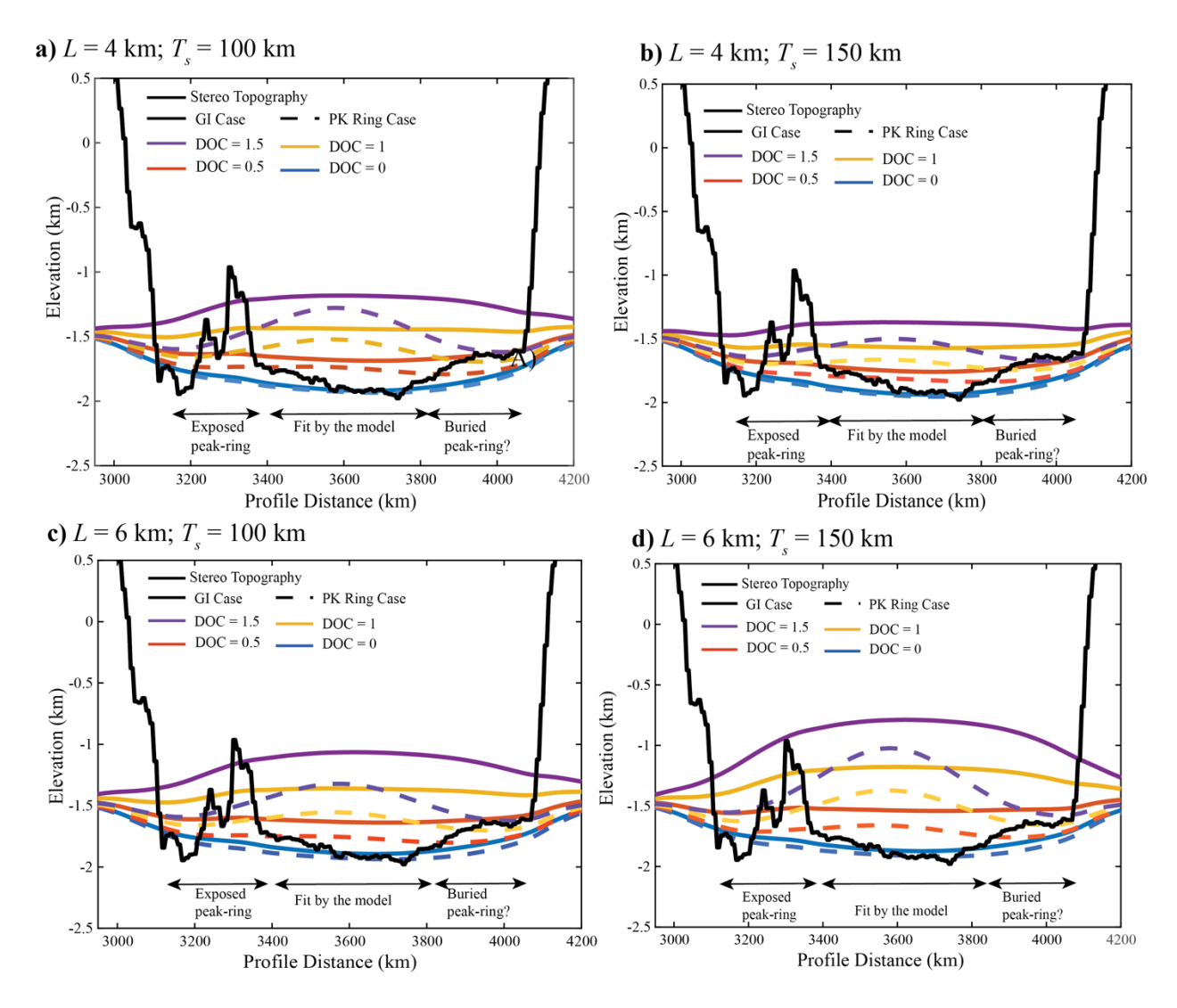


Figure 4. Cross-sectional profile of observed topography (black) compared to geoid models for a range of DOC for the giant impact basin scenario (solid colored) and the peak-/multiring basin scenario (dashed colored). Note that in computing misfits, each model geoid was shifted vertically to best align with the topography.

The RMS misfit analysis of the modeled geoids relative to the observed topography supports the results of the qualitative comparison (Figure 5). Minimum RMS misfit values range from 0.04 - 0.08 km. In general, models with low RMS misfit are those with lower DOCs for the unfilled/unloaded basin, and the RMS misfit minimum for every assumed parameter combination

is at DOC = 0. Based on the variability in the observed topography and the method described in Section 2.4 above, models that fall within 1 standard error (0.21km) of the minimum RMS misfit are considered in the most probable zone or "allowable" range. Models in the allowable range vary widely depending on the combination of assumed parameters. While the minimum RMS misfits are always at DOC=0, and the best-fit range is generally for DOC<0.7 (represented by white dashed lines in Figure 5), DOCs >1 are considered allowable in cases of a thick ice shell thickness and thin low N_2 -layer thicknesses (black dashed lines in Figure 5). There is a stronger attenuation of the gravity signature from the basal interface for a thicker shell than thinner shell, and thus models with thicker ice shells will provide reasonable fits to the topography. With all parameter combinations taken together, DOC values that span the tested range of 0 - 1.5 are considered in the allowable range even though many of these models predict concave downward geoids.

As the tested ranges of ice shell and N_2 -layer thickness exceed their likely values, we can use the preferred range of these parameters to further constrain the preferred models. For a preferred shell thickness range of 165-265 km and a N_2 thickness of 6 km, the preferred range for DOC is 0-0.5 based on the overlap with the range of best-fit models. For a preferred N_2 -layer thickness range of 4–9 km and a shell thickness of 200 km, the preferred DOC is 0-0.2. These preferred models of DOC ≤ 0.5 and the best-fit range overall for DOC ≤ 0.6 support our qualitative result that the observed topography is best matched by a mostly uncompensated basin. These results hold for both the giant impact basin scenario and the peak-/multiring basin scenario despite the difference between the scenarios in long-wavelength concavity of the compensated or over-compensated models.

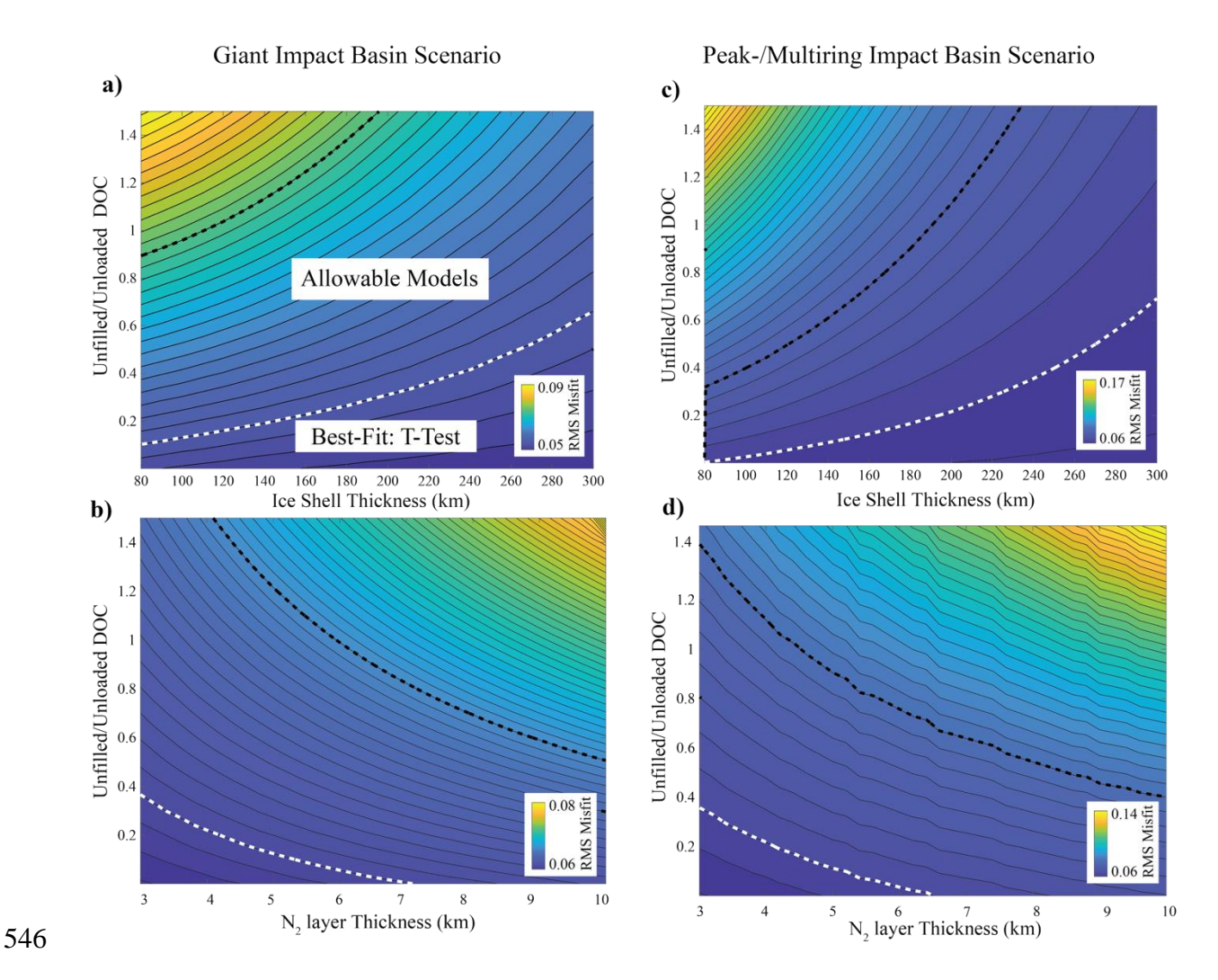


Figure 5. RMS misfit for the giant impact basin scenario (a and b) and peak-/multiring basin scenario (c and d) comparing the three main parameters of interest. For (a) and (c), L is held constant at 4 km. For (b) and (d), T_s is held constant at 200 km. Models that fall into the allowable range are within the black dashed curves. Models that fall into the best-fit range based on the t-test are within the white dashed curves.

3.3. Additional sources of mass deficit below the basin

While our results favor models of a mostly uncompensated basin today, even the fully uncompensated models do not provide a perfect fit to the geoid constraint. The observed shape of

Sputnik Planitia is more strongly concave upward than predicted by any of the models. This discrepancy suggests that there are influences from other geological processes or structures beyond what is represented in our model, resulting in a greater mass deficit in the center of the basin than the models predict. Such a mass deficit would require a negative density anomaly within the shell, as could arise from the refreezing of the uplifted ocean below the basin. As the uplifted ocean refreezes, a lens of pure water ice would form, which would have a negative density contrast if the surrounding shell contained impurities. While Pluto is most likely fully differentiated today (Robuchon and Nimmo, 2011; McKinnon et al., 2017) and the ice shell predominantly water-ice, the shell may not be pure water-ice depending on the efficiency of differentiation and its timing relative to accretion. Some silicate material or other impurities might exist within the ice shell, resulting in a higher density. Adding a lower density water-ice lens below the basin center to the uncompensated peak-ring models proves to be a better fit to the concavity of the interior of the basin with only a small density contrast between the lens and the overlying ice shell (Figure 6a). A density contrast of $\sim 100 \text{ kg/m}^3$ provides the best fit for this scenario, which would correspond to ~6% silicate impurities in the surrounding shell.

556

557

558

559

560

561

562

563

564

565

566

567

568

569

570

571

572

573

574

575

576

577

578

The observed concavity in the geoid could also be explained by an ammonia-water-ice lens below the basin. Previous studies have suggested that the subsurface ocean on Pluto may contain a small amount of ammonia, similar to icy satellites in the outer Solar System (Leliwa-Kopystynski et al., 2002; Hammond et al., 2016; Bierson et al., 2018). The mass fraction of ammonia in the ocean layer has been estimated to be on the order of 1–10% (Hammond et al., 2016; Bierson et al., 2018; Kimura and Kamata, 2020). The presence of ammonia in the ocean layer decreases the melting temperature of water-ice, improving the preservation of a subsurface ocean layer (e.g., Kimura and Kamata, 2020). As the subsurface ocean beneath the basin

refreezes and the ice-ocean interface crosses the eutectic, the refreezing ice may be contaminated by ammonia, resulting in an ammonia-water ice mixture with a lower density of ~820 kg/m³ (Martin and Binzel, 2021). Uncompensated geoid models for the peak-ring case with this structure also provide a better fit the concavity in the interior of the basin, showing a steeper concavity in this region (Figure 6b). In both cases, a lower-density lens at depth below the basin center would contribute a negative anomaly to an already uncompensated basin, increasing the concavity of the geoid anomaly and providing a better fit to the concavity of the observed topography.

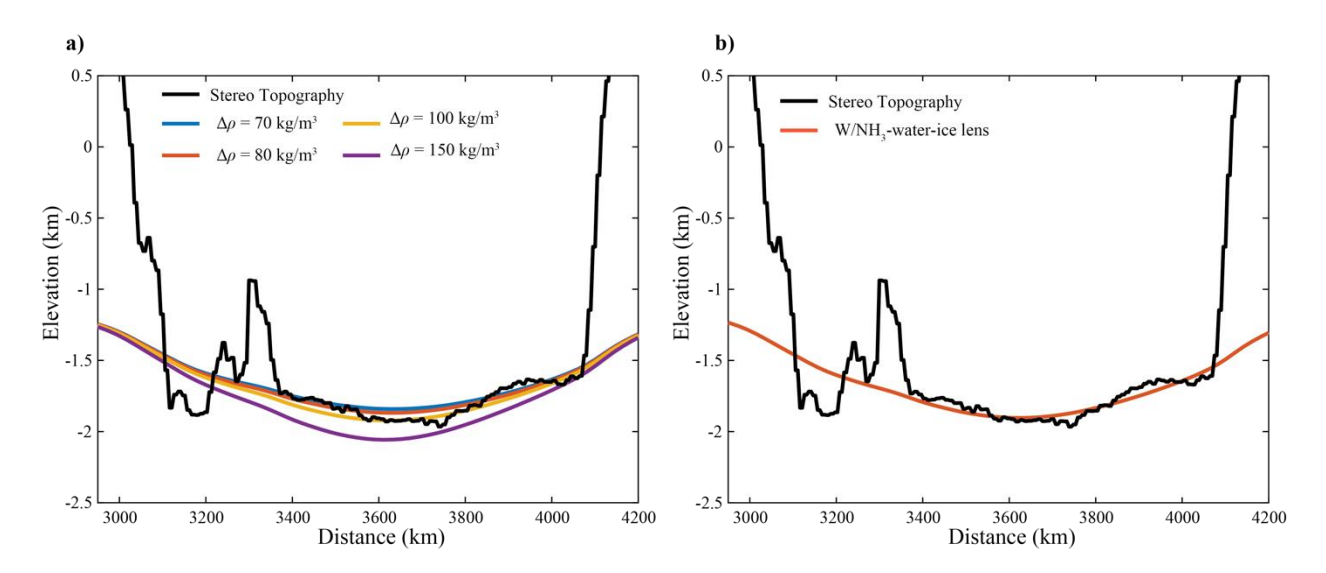


Figure 6. Cross-sectional profile of observed topography (black) compared to geoid models (colored) with DOC \sim 0 and an ice lens at depth for the multi-/peak-ring basin model. a) Geoid models of different density contrasts between a pure water-ice lens beneath a higher density ice shell. b) Geoid model containing an ammonia-water-ice lens beneath a pure water-ice shell

4. Discussion

By comparing the predicted geoid models to the observed topography of Sputnik Planitia under the assumption that its low viscosity N₂ infill conforms to the geoid, we constrain the compensation state of the basin. Our results suggest that in order to fit the concave up shape of the N₂-layer, assuming that it defines an equipotential surface, Sputnik basin is mostly uncompensated today and is likely a present-day mass deficit rather than a mass excess as previously thought (e.g., Nimmo et al., 2016; Johnson et al. 2016). Although an isostatic unfilled basin is allowable in the most extreme cases of thick shells and thin N₂ deposits, undercompensated and uncompensated basins are strongly preferred. However, after the addition of the N₂-ice fill, the mass deficit in the basin would be reduced, and partially compensated unfilled/unloaded basins (DOC~0.5) may be mass neutral today depending on the thickness of the fill and yet would still exhibit a negative geoid anomaly at the surface. If instead Sputnik basin was a mass excess/positive gravity anomaly today, as has been suggested for its past state during the reorientation of Pluto (Keane et al., 2016), then an additional process must be invoked to cause the surface of the low-viscosity N₂-layer to depart strongly from the geoid. Modeled patterns of mass loss predicted by climate models (Bertrand et al., 2017) do not explain this departure.

595

596

597

598

599

600

601

602

603

604

605

606

607

608

609

610

611

612

613

614

615

616

617

A present-day mass deficit might be expected to lead to Pluto reorienting to move the basin toward one of the poles. However, such reorientation would be resisted by the strength of the lithosphere (Matsuyama et al., 2007), particularly if one assumes the transition of the mass-deficit to have occurred later in Pluto's geodynamic history after the ice shell and elastic lithosphere had time to thicken (Hammond et al., 2016). Additionally, the initial reorientation resulted in stress in the lithosphere (Keane et al., 2016), with faulting releasing that stress down to Byerlee's law, such that the deformation upon reorientation is not simply reversible. Previous

work has shown that if Sputnik basin formed near its current location, aligned with Pluto's tidal axis, with an initial negative mass anomaly and retained that mass deficit to present-day, reorientation toward the poles is unlikely (Nimmo & Matsuyama, 2007). Similarly, sublimation of some of the N₂-layer inside the basin in the early stages of the basin's evolution would have caused only a few degrees of poleward reorientation (Johnson et al., 2021). Thus, if the basin evolved to a negative mass anomaly more recently, it may also be expected to remain in its current location. Quantifying the resistance to reorientation of Sputnik basin despite its present negative mass anomaly is an important analysis to pursue in future studies.

618

619

620

621

622

623

624

625

626

627

628

629

630

631

632

633

634

635

636

637

638

639

640

While our models cannot fully constrain structural and elastic parameters such as ice shell and elastic thickness, they do show trends within the preferred range. In general, smaller N₂-layer thicknesses and larger ice shell thicknesses within the preferred range are favored for DOC<1 As noted above, the thickness of the N₂-layer may have evolved with time in response to climate cycles and thus topographic N₂-layer loading within the basin may not have been a constant factor (Betrand et al., 2018; Johnson et al., 2021). While the variation in N₂-layer thickness may have affected the reorientation of the basin (Keane et al., 2016; Johnson et al., 2021) and the evolution of its compensation state with time, for a simple elastic lithosphere model, in which long-term viscoelastic relaxation is neglected, the present-day geoid is affected only by the present-day deposit thickness. Future observations such as a radar sounding may better constrain the N₂-layer thickness, which in turn will provide stronger constraints on our models (Howett et al., 2021). The trend towards larger shell thicknesses within the preferred range aligns well with thermal modeling that favors a thicker ice shell (e.g. Bierson et al., 2018). A thicker shell may indicate a lack of an ocean if the shell thickness is too large and extends to the ocean-core interface (Robuchon and Nimmo, 2011). However, the formation of methane

clathrates may influence the longevity of a subsurface ocean and inhibit shell thickening (Kamata et al., 2019). While our results cannot rule out the presence of an ocean, the present-day compensation state does not require an ocean. The negative geoid anomaly over the basin favors an uncompensated basin, which is compatible with either the scenario in which the present-day water layer is frozen to its basin with no remnant ocean or the scenario in which the ice-ocean interface is flat beneath the basin.

641

642

643

644

645

646

647

648

649

650

651

652

653

654

655

656

657

658

659

660

661

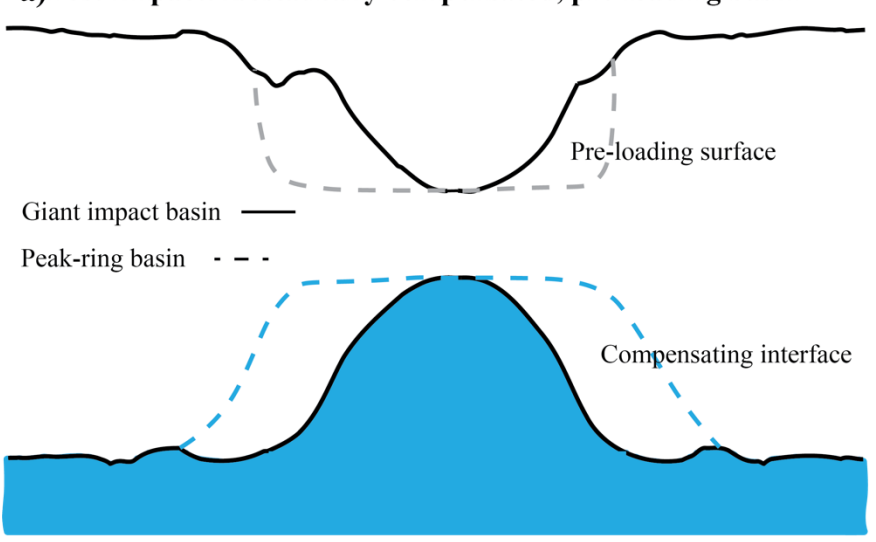
662

663

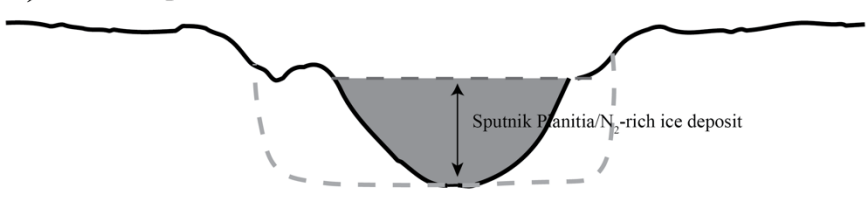
The likely present-day mass deficit over Sputnik basin is at odds with the inferred mass excess proposed to have caused reorientation of Pluto early in its history. If the basin was a mass excess in the past, the compensation state must have changed, as would be expected to occur given the thermal disequilibrium of the thinned ice shell after the impact. The basin evolution following the impact (Figure 7) would start with an unfilled Sputnik basin that was likely largely isostatically compensated by an uplifted subsurface liquid water ocean (Johnson et al., 2016; Denton et al., 2021; Nimmo et al., 2016). At this stage, Sputnik basin would exhibit a modestly negative free-air gravity anomaly at the surface due to the attenuation of the gravity anomaly arising from the compensating interface, though this is not indicative of a mass deficit. As the basin was loaded with the N₂-layer, the basin would have transitioned from isostatically compensated to overcompensated, resulting in a neutral to positive free-air gravity anomaly and a positive mass anomaly potentially leading to true polar wander. Deposition of the N₂ -layer in the basin and the resulting true polar wander occurs on tens of million-year timescale (Keane et al., 2016). Small scale deposition and sublimation within the basin may have occurred in the first few million years after reorientation (Johnson et al., 2021). As the thinned ice shell beneath the basin would have been out of equilibrium post-impact, true polar wander would likely have been followed by refreezing of the uplifted ocean. The thickening of the shell beneath basin caused it

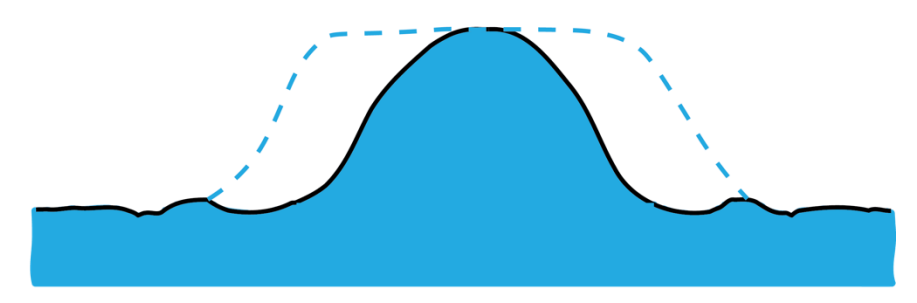
to transition from an overcompensated state to under-compensated state, even accounting for the N_2 -layer, resulting in a mass deficit and strongly negative free-air gravity and geoid anomaly today. Taken to the extreme, if the shell beneath the basin had a thickness equal to that outside of the basin, the surface depression would have a DOC< 0. Our best fit range based on the preferred range of DOC< 0.6 allows for a range of final shell thicknesses beneath the basin corresponding to a range of partially compensated basins that have not yet fully reached thermal equilibrium. A refreezing subsurface ocean beneath the basin could also contribute to the formation of the cryovolcanic structures observed in the southern tail of the basin (Martin and Binzel, 2021).

a)Post-Impact: Isostatically compensated, pre-loading basin



b) Overcompensated, filled basin





c) Present-day, uncompensated basin

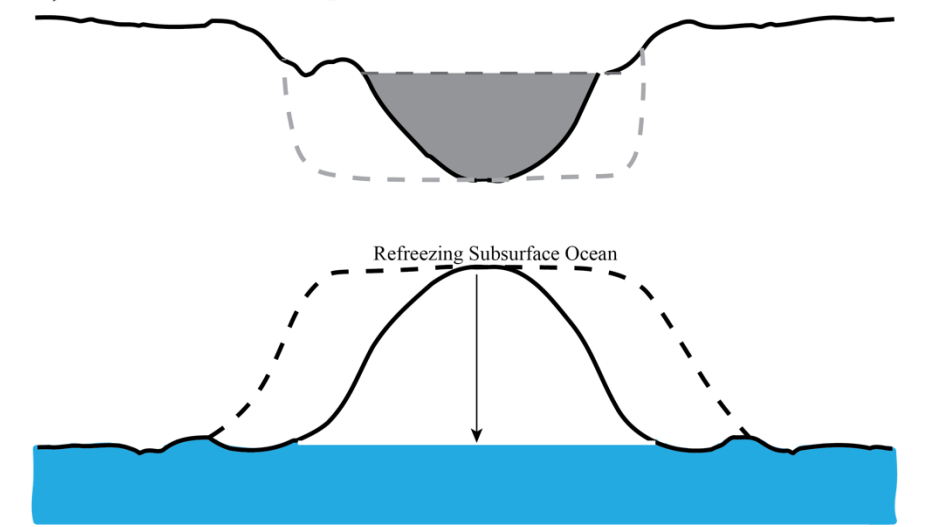


Figure 7. Proposed evolutionary trajectory of Sputnik basin from an a) isostatically compensated, unfilled basin post-impact to an b) overcompensated basin from infill of the N₂-layer to an c) uncompensated basin today after the subsurface ocean uplift refroze. Note that this schematic is not to scale, and as such, b) does not show the effect of the N₂-induced flexure of the surface and ice-ocean interface

678

679

680

681

682

683

684

685

686

687

688

689

690

691

692

693

694

695

673

674

675

676

677

There may be additional contributions to Sputnik basin's present-day mass deficit. First, Sputnik basin could have undergone viscoelastic relaxation (Kamata & Nimmo, 2014; Johnson et al., 2016; Kihoulou et al., 2022). If the thinned ice shell and associated subsurface ocean uplift experienced viscous relaxation, this would have resulted in a strong negative mass anomaly within the basin that may not have been completely offset by the positive mass anomaly generated from the N₂-layer (Denton et al., 2023). Models for Sputnik basin have demonstrated that substantial relaxation can occur for a thick (>200 km) ice shell and a pure subsurface liquid water ocean without contamination from ammonia or a subsurface layer of methane clathrates (Kihoulou et al., 2022). A layer of methane clathrates can result in a cooler shell and inhibit relaxation (Kamata et al., 2019). Viscous relaxation has been suggested for Edgeworth and Oort impact craters on Pluto, craters with diameters of ~200 km and located northwest of Sputnik basin's rim (McKinnon & Nimmo, 2023). Edgeworth crater presents topography that is characteristic of relaxation, with a shallow and slightly bowed floor, but Oort crater does not show similar topographic evidence of relaxation. Thermal studies have suggested that relaxation of both craters indicate a paleo-heat flux of greater than 10–50 mW/m² for a surface temperature of 60 K. However, if Edgeworth and Oort underwent viscous relaxation at these paleo-heat flows, it is difficult to explain why the topography of Sputnik basin has not been similarly

affected. Furthermore, these heat flows are higher than expected on Pluto (Hammond et al., 2016).

Second, a mass deficit could be a remnant from incomplete rebounding of the basin floor after the impact (Johnson et al., 2016; Denton et al. 2023). Similar mass deficits are not observed in giant impact basins on other bodies, though the pre-impact structure of Pluto differed greatly from these other bodies. However, this scenario cannot explain evidence for re-orientation of Pluto by the basin (Keane et al., 2016). There is an ~9% possibility that Sputnik basin formed at the anti-Charon point (Keane et al., 2016), in which case a mass excess is not required to reorient Pluto. Although unlikely, this scenario would allow for both a past and present mass deficit over the basin.

5. Conclusion

Sputnik basin may have been initially isostatically compensated by the uplift of a high-density ocean layer, then transitioned to a mass excess through infilling of the basin by a N_2 -layer supported by the lithosphere, inducing reorientation of Pluto to align the basin with Pluto's tidal axis. However, this evolution only constrains the mass anomaly at the time of reorientation and does not reveal the present-day state of the basin. Lacking direct gravitational data to constrain Sputnik's subsurface structure, we use a novel approach that relies on the topography of Sputnik Planitia within the basin.

Our results show that a strong, negative free-air gravity and geoid anomaly over the prefill isostatically compensated basin is predicted. This inference is at odds with other large basins in the solar system but is explained by Pluto's relatively small radius and thick shell and resulting strong attenuation of the gravity anomaly from the compensating interface when upward continued to the surface. The predicted gravitational signature of an isostatic Sputnik basin demonstrates that near-zero free-air gravity anomalies are not always a good indicator of isostasy, particularly on small bodies with thick outer crusts or shells. In our more rigorous definition of isostasy, defined as the state required to have zero net vertical displacement considering all acting loads, the geoid contribution to the load at Sputnik is found to counteract $\sim 10-15\%$ of the negative gravity anomaly, and the inclusion of the horizontal load potential counteracts $\sim 20\%$. However, the final gravity and geoid of the isostatic basin are still strongly negative even with the added load of the N_2 -layer.

Our best-fit models suggest that Sputnik basin is likely a mass deficit and at most partially compensated today. For our preferred range of N_2 -layer thicknesses and shell thicknesses, the best-fit degree of compensation for the unfilled/unloaded Sputnik basin is shown to be <0.6. Compensated and overcompensated unfilled/unloaded basin models exhibit a concave down geoid that does not reflect the observed topography of Sputnik Planitia. The best-fitting range is not particularly sensitive to whether the basin is a giant impact basin or a peak-/multiring basin, but these structures do have influence on the shape of overcompensated models. Larger shell thicknesses and thinner N_2 -layer thicknesses within the preferred range provide better fits to the geoid constraint, but our models do not fully constrain these parameters.

To reconcile our results of Sputnik basin as a likely mass deficit today with the necessity of an overcompensated basin in the past to induce true polar wander, we propose a scenario for the basin evolution. Sputnik basin may have initially been isostatically compensated with a high-density ocean layer. The basin would have evolved to an over compensated state by the infilling of the N₂-layer, resulting in reorientation of Pluto. Finally, the ice shell beneath the basin would have been out of thermal equilibrium, resulting in refreezing of the ice shell beneath the basin to

present-day. Thus, Sputnik basin would have evolved from an overcompensated state to an uncompensated state. If the refreezing uplifted subsurface ocean resulted in an ice lens of lower density than the surroundings, either because it contained a water-ammonia-ice mixture or because the surrounding shell was contaminated by silicates, the fit to the concavity of the topography could be improved. Future thermal modeling studies of the basin would be useful to test this scenario. Taken together, constraints on the geoid over the basin, models of basin formation, and models of thermal and viscous evolution of the basin contribute to better constrain the present-day structure and compensation state of Sputnik basin, with important implications for the possible existence, longevity, and evolution of a subsurface ocean on Pluto.

751

752

753

742

743

744

745

746

747

748

749

750

Acknowledgements

- This work was funded by Grant 80NSSC19K0819 from the NASA NFDAP program to J.C.
- Andrews-Hanna and by Grant 80NSSC22K1366 from the NASA FINESST program to S.A.
- 755 Moruzzi

756

757

Open Research

- 758 Pluto Digital Elevation Model (Schenk et al., 2018) projected at 300 m/pixel used in this study
- can be accessed through the Cartography and Imaging Science node of the PDS through the
- 760 Astropedia website at this link:
- https://astrogeology.usgs.gov/search/map/pluto new horizons lorri mvic global dem 300m
- Models and figures were made using MATLAB R2024 version 24.1.0 and Python 3.13. Models
- and code for calculating the geoid over Sputnik basin (Moruzzi, 2025) can be accessed/is
- archived in a Zenodo repository: https://doi.org/10.5281/zenodo.15103047. The original thin-

765 shell deformation model from Broquet (2022) is a publicly available Python code and can be 766 accessed/ is archived on GitHub: https://github.com/AB-Ares/Displacement strain planet and in 767 a Zenodo repository: http://doi.org/10.5281/zenodo.4916799 768 769 770 References 771 Andersen, O. B., & Knudsen, P. (1998). Global marine gravity field from the ERS-1 and Geosat 772 geodetic mission altimetry. Journal of Geophysical Research: Oceans, 103(C4), 8129– 773 8137. 774 Andrews-Hanna, J. C. (2013). The origin of the non-mare mascon gravity anomalies in lunar 775 basins. *Icarus*, 222(1), 159–168. 776 Andrews-Hanna, J. C., & Zuber, M. T. (2010). Elliptical craters and basins on the terrestrial 777 planets. Geological Society of America Special Papers, 465, 1-13. 778 Andrews-Hanna, J. C., Zuber, M. T., & Banerdt, W. B. (2008). The Borealis basin and the origin 779 of the martian crustal dichotomy. *Nature*, 453(7199), 1212-1215. 780 Banerdt, W. B. (1986). Support of long-wavelength loads on Venus and implications for internal 781 structure. *Journal of Geophysical Research: Solid Earth*, 91(B1), 403-419. 782 Banerdt, W. B., & Golombek, M. P. (1990). The evolution of Tharsis: implications of gravity, 783 topography, and tectonics. Lunar and Planetary Inst., Scientific Results of the NASA-784 Sponsored Study Project on Mars: Evolution of Volcanism, Tectonics, and Volatiles. 785 Bertrand, T., Forget, F., Umurhan, O. M., Grundy, W. M., Schmitt, B., Protopapa, S., ... & Olkin, 786 C. B. (2018). The nitrogen cycles on Pluto over seasonal and astronomical 787 timescales. Icarus, 309, 277-296.

- 788 Beuthe, M. (2021). Isostasy with Love-I: elastic equilibrium. Geophysical Journal
- 789 *International*, 225(3), 2157-2193.
- 790 Beuthe, M. (2008). Thin elastic shells with variable thickness for lithospheric flexure of one-
- plate planets. *Geophysical Journal International*, 172(2), 817-841.
- Beuthe, M., Rivoldini, A., & Trinh, A. (2016). Enceladus's and Dione's floating ice shells
- supported by minimum stress isostasy. *Geophysical Research Letters*, 43(19), 10-088.
- 794 Bierson, C. J., Nimmo, F., & McKinnon, W. B. (2018). Implications of the observed Pluto-
- 795 Charon density contrast. *Icarus*, *309*, 207-219.
- 796 Bjonnes, E., Johnson, B. C., & Andrews-Hanna, J. C. (2023). Basin Crustal Structure at the
- 797 Multiring Basin Transition. *Journal of Geophysical Research: Planets*, 128(4),
- 798 e2022JE007507.
- 799 Broquet, A. (2022). Displacement strain planet: Version 0.3.1. [Software]. Zenodo.
- 800 http://doi.org/10.5281/zenodo.4916799
- Broquet, A., & Andrews-Hanna, J. C. (2023a). Plume-induced flood basalts on Hesperian Mars:
- An investigation of Hesperia Planum. *Icarus*, 391, 115338.
- Broquet, A., & Andrews-Hanna, J. C. (2024). The moon before mare. *Icarus*, 408, 115846.
- 804 Conrad, J. W., Nimmo, F., Schenk, P. M., McKinnon, W. B., Moore, J. M., Beddingfield, C. B.,
- 805 ... & Ennico, K. (2019). An upper bound on Pluto's heat flux from a lack of flexural
- response of its normal faults. *Icarus*, 328, 210-217.
- Dahlen, F. A. (1982). Isostatic geoid anomalies on a sphere. *Journal of Geophysical Research*:
- 808 Solid Earth, 87(B5), 3943-3947.
- Denton, C. A., Gosselin, G. J., Freed, A. M., & Johnson, B. C. (2023). The formation and
- evolution of Pluto's Sputnik basin prior to nitrogen ice fill. *Icarus*, 398, 115541.

- Ding, M., & Zhu, M. H. (2022). Effects of regional thermal state on the crustal annulus
- relaxation of lunar large impact basins. *Journal of Geophysical Research*:
- 813 *Planets*, 127(3), e2021JE007132.
- Freed, A. M., Johnson, B. C., Blair, D. M., Melosh, H. J., Neumann, G. A., Phillips, R. J., ... &
- Zuber, M. T. (2014). The formation of lunar mascon basins from impact to contemporary
- form. Journal of Geophysical Research: Planets, 119(11), 2378-2397.
- Hammond, N. P., Barr, A. C., & Parmentier, E. M. (2016). Recent tectonic activity on Pluto
- driven by phase changes in the ice shell. *Geophysical Research Letters*, 43(13), 6775-6782.
- Hammond, N. P., Parmenteir, E. M., & Barr, A. C. (2018). Compaction and Melt Transport in
- Ammonia-Rich Ice Shells: Implications for the Evolution of Triton. Journal of
- 821 *Geophysical Research: Planets*, *123*(12), 3105-3118.
- Hemingway, D. J., & Matsuyama, I. (2017). Isostatic equilibrium in spherical coordinates and
- implications for crustal thickness on the Moon, Mars, Enceladus, and elsewhere.
- 824 *Geophysical Research Letters*, *44*(15), 7695–7705.
- Howett, C. J., Robbins, S. J., Holler, B. J., Hendrix, A., Fielhauer, K. B., Perry, M. E., ... &
- Young, L. A. (2021). Persephone: A Pluto-system Orbiter and Kuiper Belt Explorer. The
- 827 Planetary Science Journal, 2(2), 75.
- Johnson, B. C., Andrews-Hanna, J. C., Collins, G. S., Freed, A. M., Melosh, H. J., & Zuber, M.
- 829 T. (2018). Controls on the formation of lunar multiring basins. Journal of Geophysical
- 830 Research: Planets, 123(11), 3035-3050.
- Johnson, B. C., Bowling, T. J., Trowbridge, A. J., & Freed, A. M. (2016). Formation of the
- 832 Sputnik Planum basin and the thickness of Pluto's subsurface ocean. Geophysical
- 833 Research Letters, 43(19), 10-068.

- Johnson, P. E., Keane, J. T., Young, L. A., & Matsuyama, I. (2021). New Constraints on Pluto's
- Sputnik Planitia Ice Sheet from a Coupled Reorientation–Climate Model. *The Planetary*
- 836 *Science Journal*, 2(5), 194.
- Kamata, S., & Nimmo, F. (2014). Impact basin relaxation as a probe for the thermal history of
- Pluto. Journal of Geophysical Research: Planets, 119(10), 2272-2289.
- 839 Kanamaru, M., Sasaki, S., & Wieczorek, M. (2019). Density distribution of asteroid 25143
- Itokawa based on smooth terrain shape. *Planetary and Space Science*, 174, 32-42.
- Keane, J. T., Matsuyama, I., Kamata, S., & Steckloff, J. K. (2016). Reorientation and faulting of
- Pluto due to volatile loading within Sputnik Planitia. *Nature*, 540(7631), 90-93.
- Kihoulou, M., Kalousová, K., & Souček, O. (2022). Evolution of Pluto's impact-deformed ice
- 844 shell below sputnik planitia basin. Journal of Geophysical Research: Planets, 127(6),
- 845 e2022JE007221.
- 846 Kimura, Jun, and Shunichi Kamata. "Stability of the subsurface ocean of Pluto." *Planetary and*
- *Space Science* 181 (2020): 104828
- 848 Leliwa-Kopystyński, J., Maruyama, M., & Nakajima, T. (2002). The water–ammonia phase
- diagram up to 300 MPa: Application to icy satellites. *Icarus*, 159(2), 518-528.
- Martin, C. R., & Binzel, R. P. (2021). Ammonia-water freezing as a mechanism for recent
- 851 cryovolcanism on Pluto. *Icarus*, *356*, 113763.
- Matsuyama, I., Nimmo, F., & Mitrovica, J. X. (2007). Reorientation of planets with lithospheres:
- The effect of elastic energy. *Icarus*, 191(2), 401-412.
- McGovern, P. J., White, O. L., & Schenk, P. M. (2021). Tectonism and Enhanced Cryovolcanic
- Potential Around a Loaded Sputnik Planitia Basin, Pluto. Journal of Geophysical
- 856 Research: Planets, 126(12), e2021JE006964.

- McKinnon, W. B., Nimmo, F., Wong, T., Schenk, P. M., White, O. L., Roberts, J. H., ... & Smith,
- K. E. (2016). Convection in a volatile nitrogen-ice-rich layer drives Pluto's geological
- 859 vigour. *Nature*, 534(7605), 82-85.
- McKinnon, W. B., Stern, S. A., Weaver, H. A., Nimmo, F., Bierson, C. J., Grundy, W. M., ... &
- 861 Smith, K. E. (2017). Origin of the Pluto-Charon system: Constraints from the New
- 862 Horizons flyby. *Icarus*, 287, 2-11.
- Melosh, H. J., Freed, A. M., Johnson, B. C., Blair, D. M., Andrews-Hanna, J. C., Neumann, G.
- 864 A., ... & Zuber, M. T. (2013). The origin of lunar mascon basins. Science, 340(6140), 1552-
- 865 1555.
- Moore, J. M., McKinnon, W. B., Spencer, J. R., Howard, A. D., Schenk, P. M., Beyer, R. A., ... &
- New Horizons Science Team. (2016). The geology of Pluto and Charon through the eyes
- of New Horizons. *Science*, *351*(6279), 1284-1293.
- 869 Moruzzi (2025). CompensationState SputnikBasin. [Software]. Zenodo.
- 870 <u>https://doi.org/10.5281/zenodo.15103047</u>
- Moruzzi, S.A., Andrews-Hanna, J.C. & Schenk, P. (2023). Pluto's Sputnik Basin as a Peak-Ring
- or Multiring Basin: A Comparative Study. *Icarus*, 115721
- Neumann, G. A., Zuber, M. T., Wieczorek, M. A., Head, J. W., Baker, D. M. H., Solomon, S. C.,
- Smith, D. E., Lemoine, F. G., Mazarico, E., Sabaka, T. J., Goossens, S. J., Melosh, H. J.,
- Phillips, R. J., Asmar, S. W., Konopliv, A. S., Williams, J. G., Sori, M. M., Soderblom, J.
- M., Miljković, K., ... Kiefer, W. S. (2015). Lunar impact basins revealed by Gravity
- 877 Recovery and Interior Laboratory measurements. *Science Advances*, 1(9), e1500852.
- Nimmo, F., & McKinnon, W. B. (2021). Geodynamics of Pluto. See Stern, et al.

- Nimmo, F., Hamilton, D. P., McKinnon, W. B., Schenk, P. M., Binzel, R. P., Bierson, C. J., ... &
- Smith, K. E. (2016). Reorientation of Sputnik Planitia implies a subsurface ocean on
- 881 Pluto. *Nature*, 540(7631), 94-96.
- Potter, R. W. (2015). Investigating the onset of multi-ring impact basin formation. *Icarus*, 261,
- 883 91- 99.
- Ritzer, J. A., & Hauck II, S. A. (2009). Lithospheric structure and tectonics at Isidis Planitia,
- 885 Mars. *Icarus*, 201(2), 528-539.
- Robuchon, G., & Nimmo, F. (2011). Thermal evolution of Pluto and implications for surface
- tectonics and a subsurface ocean. *Icarus*, 216(2), 426-439.
- Schenk, P. M., Beyer, R. A., McKinnon, W. B., Moore, J. M., Spencer, J. R., White, O. L., ... &
- Olkin, C. (2018). Basins, fractures and volcanoes: Global cartography and topography of
- Pluto from New Horizons. *Icarus*, 314, 400–433.
- Scott, T. A. (1976). Solid and liquid nitrogen. *Physics Reports*, 27(3), 89-157.
- 892 Searls, M. L., Banerdt, W. B., & Phillips, R. J. (2006). Utopia and Hellas basins, Mars: Twins
- 893 separated at birth. *Journal of Geophysical Research: Planets*, 111(E8).
- 894 Sleep, N. H., & Phillips, R. J. (1979). An isostatic model for the Tharsis
- ProvinceMars. Geophysical Research Letters, 6(10), 803-806.
- 896 Solomon, S. C., & Head, J. W. (1980). Lunar mascon basins: Lava filling, tectonics, and
- 897 evolution of the lithosphere. Reviews of Geophysics, 18(1), 107-141
- 898 Stern, S. A., Bagenal, F., Ennico, K., Gladstone, G. R., Grundy, W. M., McKinnon, W. B., ... &
- 899 Zangari, A. M. (2015). The Pluto system: Initial results from its exploration by New
- 900 Horizons. *Science*, *350*(6258).

901 Trowbridge, A. J., Johnson, B. C., Freed, A. M., & Melosh, H. J. (2020). Why the lunar South 902 Pole-Aitken Basin is not a mascon. Icarus, 352, 113995. 903 Trowbridge, A. J., Melosh, H. J., Steckloff, J. K., & Freed, A. M. (2016). Vigorous convection as 904 the explanation for Pluto's polygonal terrain. *Nature*, 534(7605), 79–81. 905 Turcotte, D. L., & Schubert, G. (2002). Geodynamics. "Elasticity and Flexure" pp 105-131, 906 Cambridge university press. 907 Umurhan, O. M., Howard, A. D., Moore, J. M., Earle, A. M., White, O. L., Schenk, P. M., ... & 908 Young, L. A. (2017). Modeling glacial flow on and onto Pluto's Sputnik 909 Planitia. Icarus, 287, 301-319 910 White, O. L., Schenk, P. M., & Dombard, A. J. (2013). Impact basin relaxation on Rhea and 911 Iapetus and relation to past heat flow. *Icarus*, 223(2), 699-709. 912 Wieczorek, M. A., & Phillips, R. J. (1998). Potential anomalies on a sphere: Applications to the 913 thickness of the lunar crust. Journal of Geophysical Research: Planets, 103(E1), 1715-914 1724.